


## Article

# Identification and Control of Flexible Joint Robots Based on a Composite-Learning Optimal Bounded Ellipsoid Algorithm and Prescribe Performance Control Technique

Xianyan Li <sup>1</sup>, Dongdong Zheng <sup>1,2,\*</sup>, Kai Guo <sup>3,\*</sup>  and Xuemei Ren <sup>1</sup>

<sup>1</sup> School of Automation, Beijing Institute of Technology, Beijing 100811, China; lixianyan2022@163.com (X.L.); xmren@bit.edu.cn (X.R.)

<sup>2</sup> China North Artificial Intelligence & Innovation Research Institute, Beijing 100072, China

<sup>3</sup> School of Mechanical Engineering, Shandong University, Jinan 250061, China

\* Correspondence: ddongzheng@outlook.com (D.Z.); kaiguo@sdu.edu.cn (K.G.)

**Abstract:** This paper presents an indirect adaptive neural network (NN) control algorithm tailored for flexible joint robots (FJR), aimed at achieving desired transient and steady-state performance. To simplify the controller design process, the original higher-order system is decomposed into two lower-order subsystems using the singular perturbation technique (SPT). NNs are then employed to reconstruct the aggregated uncertainties. An adaptive prescribed performance control (PPC) strategy and a continuous terminal sliding mode control strategy are introduced for the reduced slow subsystem and fast subsystem, respectively, to guarantee a specified convergence speed and steady-state accuracy for the closed-loop system. Additionally, a composite-learning optimal bounded ellipsoid algorithm (OBE)-based identification scheme is proposed to update the NN weights, where the tracking errors of the reduced slow and fast subsystems are integrated into the learning algorithm to enhance the identification and tracking performance. The stability of the closed-loop system is rigorously established using the Lyapunov approach. Simulations demonstrate the effectiveness of the proposed identification and control schemes.

**Keywords:** optimal bounded ellipsoid; flexible joint robots; prescribed performance control; singular perturbation technique; neural networks; composite learning



**Citation:** Li, X.; Zheng, D.; Guo, K.; Ren X. Identification and Control of Flexible Joint Robots Based on a Composite-Learning Optimal Bounded Ellipsoid Algorithm and Prescribe Performance Control Technique. *Appl. Sci.* **2024**, *14*, 4030. <https://doi.org/10.3390/app14104030>

Academic Editors: George Mylonas and Marco Troncosi

Received: 29 February 2024

Revised: 13 April 2024

Accepted: 7 May 2024

Published: 9 May 2024



**Copyright:** © 2024 by the authors. Licensee MDPI, Basel, Switzerland. This article is an open access article distributed under the terms and conditions of the Creative Commons Attribution (CC BY) license (<https://creativecommons.org/licenses/by/4.0/>).

## 1. Introduction

In today's complex work environment, where human–robot interaction has become increasingly frequent, a diverse range of robots has emerged to cater to distinct implementation scenarios. Among these robots, FJR have garnered significant attention due to their inherent compliance, which enhances the safety of human interactions [1]. Typically, FJR comprise motors with load links, connected via low-stiffness flexible couplings. This joint elasticity allows FJR to be modeled as a two-mass system. To effectively control these systems, numerous control methods have been proposed in the academic literature. For instance, Zhu et al. [2] combined command filtering with adaptive fuzzy control methods to control FJR with time-varying full-state constraints. Xu et al. [3] elaborated on how to integrate event-triggered control with adaptive neural networks to design a control strategy, aiming to achieve precise tracking control of FJR. Jerónimo et al. [4] combined a PID-type control strategy with motor position measurement information to achieve precise control of FJR.

In practical scenarios, it is crucial to confine the tracking error within a predefined range. To this end, PPC has garnered significant attention from researchers [5–7]. Ma, for instance, introduced an adaptive fuzzy control approach for single-link flexible-joint robotic manipulators, leveraging PPC to ensure transient performance guarantees [8]. Furthermore, FJR can achieve desired impedance against external contact forces and superior

position tracking in free motion, thanks to robust prescribed performance position tracking controllers [9]. However, it is worth noting that the aforementioned control methods often rely on backstepping or dynamic surface control techniques, which are renowned for their intricate and repetitive design procedures. Consequently, their application in real high-order FJRs remains limited.

In FJRs, the position and velocity of links exhibit slower time-scale variations, whereas the position and velocity of motors undergo faster dynamics. This characteristic allows the overall system dynamic equations to be recast into a standard singularly perturbed form, facilitating the utilization of SPT to simplify controller design. Kim et al. [10], for instance, applied SPT to decompose the higher-order model of a serial elastic actuator into two lower-order models. Subsequently, they developed a second-order sliding mode control law for each lower-order model, ensuring semi-global exponential stability. Another study by Sun et al. [11] introduced a nonlinear hybrid control scheme for a redundant parallel robot system, leveraging SPT and Tikhonov's theorem to achieve both trajectory tracking and vibration suppression. Chen et al. proposed a prescribed performance controller for FJRs with exogenous disturbances, incorporating SPT and a time-varying tangent barrier Lyapunov function to expand the initial error constraint boundary [12]. However, these methods fail to identify and compensate for unknown dynamics in FJRs, resulting in relatively large control errors.

To address the challenges posed by unknown nonlinear dynamics in practical systems, NNs have been extensively employed due to their remarkable universal approximation capabilities [13–17]. In the development of NN-based adaptive control methods, the algorithm for identifying NN weights plays a crucial role, as it profoundly affects both the tracking performance and the robustness of the closed-loop system [18]. NN-based adaptive control methods can be categorized into two main branches: direct adaptive control methods [19–21] and indirect adaptive control methods [22]. Direct adaptive control primarily relies on gradient-descent-based updating laws for online identification of unknown controller parameters. However, these methods may not yield satisfactory identification results [23]. Consequently, indirect adaptive control has garnered significant attention since it offers more advanced identification algorithms. A traditional approach in this domain is the identification algorithm based on the Kalman filter, which characterizes uncertainty through a noise signal with a predefined probability density function [24]. However, the limited capability of this algorithm in handling nonlinear systems restricts its utilization in specific application scenarios [25].

The set-membership identification approach ensures that the parameters belong to specific sets, offering increased flexibility in addressing intricate problems. Among the various set-membership identification methods, the OBE algorithm stands out as the most prominent. The OBE algorithm has significant importance in the realms of system identification and adaptive control, serving as an effective and precise tool for the estimation of unknown system parameters [26]. This iterative technique incrementally shrinks the volume of an ellipsoid to yield the optimal parameter estimate. Notably, ellipsoids are employed in this context to demarcate predefined sets [27,28]. The learning gain matrix in the OBE algorithm exhibits dynamic characteristics, with an upper bound that prevents explosions in scenarios of inadequate excitation and a lower bound that guarantees robust identification performance for time-varying parameters. The OBE algorithm has been studied extensively in the literature. For example, Davila et al. proposed a novel dynamic sliding mode control design scheme by combining sliding mode control with the attracting ellipsoid method, enabling the system state to rapidly enter and maintain the sliding surface during the dynamic process [29]. Cao et al. introduced a directional forgetting algorithm that discards outdated data based on the informational content across various directions, above and below the bounded information matrix [30]. Ordaz et al. developed an adaptive state estimator and a robust output control for a class of uncertain nonlinear systems, which enables the system to maintain stability and performance in the presence of uncertainty and disturbances, and the feedback gains  $K$ ,  $L$  can be updated online based on the attractive

ellipsoid method [31]. Guo et al. proposed an efficient OBE identification algorithm that ensures deterministic upper and lower bounds for the learning gain matrix [13,32]. Applications of OBE-based algorithms for the identification of singularly perturbed systems have been detailed in [33,34]. However, it is crucial to note that these papers rely solely on identification errors for updating NN weights. As highlighted in [22], incorporating both identification and tracking errors in weight updating laws enhances NN training outcomes. Therefore, it is advisable to incorporate the tracking error into a composite learning algorithm to further bolster identification performance.

To tackle the aforementioned challenges, this paper introduces a novel identification and control algorithm tailored for the FJR. The key contributions of this work are outlined below:

- An adaptive prescribed performance controller for the FJR is formulated, leveraging the SPT framework and continuous terminal sliding mode control technique. This simplifies the controller design process and ensures that the transient and steady-state behavior meets the pre-established specifications.
- A composite-learning OBE-based identification algorithm is introduced, aiming to boost NN training performance by incorporating both identification and tracking errors.

The subsequent sections of this paper are organized as follows: Section 2 presents preliminary information and demonstrates how the original high-order FJR can be decoupled into two lower-order subsystems using SPT. Section 3 introduces an NN-based terminal sliding mode PPC for the simplified subsystems. The identification algorithm is presented in Section 4. Simulation results are presented in Section 5 to demonstrate the efficacy of the proposed control method, and Section 6 concludes the paper with final remarks.

## 2. Preliminaries and Problem Formulation

An FJR can be described by the following dynamic model [35]:

$$M(q)\ddot{q} + C(q, \dot{q})\dot{q} + D(\dot{q}) + G(q) + \tau_d = K(\theta - q) \quad (1a)$$

$$J\ddot{\theta} + K(\theta - q) = u, \quad (1b)$$

where  $q(t) \in \mathbb{R}^n$ ,  $\dot{q}(t) \in \mathbb{R}^n$  are the angular position and velocity of the joints, and  $\theta \in \mathbb{R}^n$  and  $\dot{\theta} \in \mathbb{R}^n$  represent the angular position and velocity of the motors.  $M(q) \in \mathbb{R}^{n \times n}$ ,  $C(q, \dot{q}) \in \mathbb{R}^n$ ,  $D(\dot{q}) \in \mathbb{R}^n$ ,  $G(q) \in \mathbb{R}^n$ ,  $u \in \mathbb{R}^n$  represents the inertia matrix, the centripetal/Coriolis matrix, the friction torque vector, the gravity torque vector, and the system input vector, respectively.  $\tau_d \in \mathbb{R}^n$  is a bounded aggregate disturbance term that encompasses various sources of uncertainty, including inaccuracies in the model, uncaptured dynamics, and external perturbations.  $K \in \mathbb{R}^{n \times n}$  is a diagonal matrix representing the stiffness of the spring between the motor and the link, and  $J \in \mathbb{R}^{n \times n}$  is a diagonal matrix representing the inertia of the motors.

Denote  $H_r(q, \dot{q}) = C(q, \dot{q})\dot{q} + D\dot{q} + G(q)$ ,  $\tau_1 = K(\theta(t) - q(t))$ . Considering the fact that the torque  $\tau_1$  generated by the spring changes much faster than the position of the link  $q$ , then by defining  $K = K_0/\varepsilon^2$ , where  $\varepsilon$  is a small parameter, and  $K_0 \in \mathbb{R}^{n \times n}$  is a positive-definite diagonal matrix, we can use a singular perturbation model to describe the FJR as

$$M(q)\ddot{q} + H_r(q, \dot{q}) + \tau_d = \tau_1 \quad (2a)$$

$$\varepsilon^2 J\ddot{\tau}_1 + K_0\tau_1 = K_0(u - J\ddot{q}). \quad (2b)$$

**Remark 1.** In control systems theory, the singular perturbation model is extensively employed to describe dynamical systems, where certain state derivatives are scaled by a small positive parameter  $\varepsilon$ . These states scaled by  $\varepsilon$  are known as fast states, while the remaining states are classified as slow. A decrease in  $\varepsilon$  typically correlates with accelerated changes in the fast states. For such systems, the singular perturbation technique serves as a valuable tool for order reduction and controller simplification [36]. Although there is no standardized approach for selecting  $\varepsilon$ , for flexible joint

robots, it is customary to choose  $\varepsilon$  inversely proportional to the square root of joint stiffness [37]. As joint stiffness  $K$  increases,  $\varepsilon$  decreases, resulting in faster torque  $\tau_1$  changes. In particular, as  $K$  approaches infinity,  $\varepsilon$  tends to zero, causing instantaneous torque  $\tau_1$  changes, effectively transforming the flexible joint robot into a rigid joint robot.

Substituting (2a) into (2b), one obtains

$$\varepsilon^2 J \ddot{\tau}_1 + K_0 \tau_1 = K_0 u - K_0 J M^{-1} (\tau_1 - \tau_d - H_r). \quad (3)$$

Multiplying both sides of (3) with  $J^{-1}$ , one obtains

$$\varepsilon^2 \ddot{\tau}_1 = K_0 \left( J^{-1} (u - \tau_1) + M^{-1} (H_r + \tau_d - \tau_1) \right). \quad (4)$$

Let  $x_1 := q$ ,  $x_2 := \dot{q}$ ,  $\tau_2 := \varepsilon \dot{\tau}_1$ , then, (2) can be written as

$$\dot{x}_1 = x_2 \quad (5a)$$

$$\dot{x}_2 = M^{-1} (\tau_1 - H_r - \tau_d) \quad (5b)$$

$$\varepsilon \dot{\tau}_1 = \tau_2 \quad (5c)$$

$$\varepsilon \dot{\tau}_2 = K_0 \left( J^{-1} (u - \tau_1) + M^{-1} (H_r + \tau_d - \tau_1) \right). \quad (5d)$$

Because  $\tau_d$  is unknown, a three-layer neural network is adopted to approximate  $-M^{-1}\tau_d$  as:

$$-M^{-1}\tau_d = W^{*T}\Phi(Z) + \zeta, \quad (6)$$

where  $W^* = [W_1^*, W_2^*, \dots, W_n^*] \in \mathbb{R}^{N \times n}$  is a matrix of NN weights,  $W_i^* = [w_i^{*1}, w_i^{*2}, \dots, w_i^{*N}]^T \in \mathbb{R}^N$ ,  $N \in \mathbb{Z}^+$  is the number of neurons used in the hidden layer,  $Z = [z_1, \dots, z_N] = V\mathbf{x}$ , with  $\mathbf{x} = [x_1^T, x_2^T]^T$  being the input of the NNs, and  $V \in \mathbb{R}^{N \times 2n}$  the weights between the input and the hidden layer,  $\Phi = [\phi_1, \phi_2, \dots, \phi_N]^T \in \mathbb{R}^N$  is a vector of regression functions,  $\phi_k : \mathbb{R} \mapsto \mathbb{R}^+$  with  $k = 1, \dots, N$  is a sigmoid function modeled by  $\phi_k = 1/(1 + e^{-z_k})$ , and  $\zeta \in \mathbb{R}^n$  is the approximation error of the NN.

Using (6), the system (5) can be written as

$$\dot{x}_1 = x_2 \quad (7a)$$

$$\dot{x}_2 = M^{-1} (\tau_1 - H_r) + W^{*T}\Phi + \zeta \quad (7b)$$

$$\varepsilon \dot{\tau}_1 = \tau_2 \quad (7c)$$

$$\varepsilon \dot{\tau}_2 = K_0 \left( J^{-1} (u - \tau_1) + M^{-1} (H_r - \tau_1) - W^{*T}\Phi - \zeta \right). \quad (7d)$$

To apply the singular perturbation technique, one can first set  $\varepsilon=0$  in (7d) and neglect the unknown  $W^{*T}\Phi$  and  $\zeta$ ; then,  $\tau_1$  has a unique isolated root

$$\begin{aligned} \tau_1^* &= h(x, t) = (M^{-1} + J^{-1})^{-1} (J^{-1} u_s + M^{-1} H_r) \\ &= a u_s + b H_r, \end{aligned} \quad (8)$$

where  $u_s$  is the slow control component of  $u$  when  $\varepsilon = 0$ , and  $a = (M^{-1} + J^{-1})^{-1} J^{-1}$ ,  $b = (M^{-1} + J^{-1})^{-1} M^{-1}$ .

Replace  $\tau_1$  with  $\tau_1^*$  in (7), the reduced slow subsystem can be obtained as

$$\dot{x}_1 = x_2 \quad (9a)$$

$$\dot{x}_2 = M^{-1} \left( a u_s + (b - I) H_r \right) + W^{*T}\Phi + \zeta. \quad (9b)$$

Define a new state variable  $\Lambda = \tau_1 - h(x, t)$ ; the fast dynamics in (7) can be written as

$$\varepsilon \dot{\Lambda} = \tau_2 - \varepsilon \dot{h}(x, t) \quad (10a)$$

$$\varepsilon \dot{\tau}_2 = K_0 \left( J^{-1}(u - \tau_1) + M^{-1}(H_r - \tau_1) - W^{*T} \Phi - \zeta \right). \quad (10b)$$

Define a “stretched” time variable  $t_\varepsilon := \frac{t}{\varepsilon}$ . Setting  $\varepsilon=0$  freezes the variables  $x$  and  $t$  at  $x_0$  and 0, respectively, so that  $h(x, t)$  is constant at the fast time scale  $t_\varepsilon$ . Then, substituting  $\tau_1 = \Lambda + h(x, t)$  with  $\dot{h} = 0$  into (10) and changing the consequent expression into the fast time scale  $t_\varepsilon$ , one obtains

$$\frac{d\Lambda}{dt_\varepsilon} = \tau_2 \quad (11a)$$

$$\begin{aligned} \frac{d\tau_2}{dt_\varepsilon} = & K_0 J^{-1} u + K_0 M^{-1} H_r - K_0 (W^{*T} \Phi + \zeta) \\ & - K_0 (M^{-1} + J^{-1}) (\Lambda + h(x, t)). \end{aligned} \quad (11b)$$

Applying (8) into the above equations and setting  $\varepsilon = 0$ , the *reduced fast subsystem* can be obtained as

$$\frac{d\Lambda}{dt_\varepsilon} = \tau_2 \quad (12a)$$

$$\frac{d\tau_2}{dt_\varepsilon} = K_0 \left( J^{-1} u_f - (M^{-1} + J^{-1}) \Lambda - (W^{*T} \Phi + \zeta) \right), \quad (12b)$$

where  $u_f := u - u_s$ .

### 3. Continuous Terminal Sliding Mode Control of the Flexible Joint Robotic Manipulator

This paper aims to ensure the angular position of joints,  $q$ , accurately tracking a designated reference,  $q_d$ , while meeting pre-specified transient and steady-state performance criteria. Leveraging the singular perturbation technique (SPT), the high-order singular perturbation model (7) is successfully decomposed into two lower-order subsystems: (9) and (12). According to Tikhonov’s theory [36], controlling these reduced-order subsystems suffices to solve the trajectory tracking problem for the original system, thereby simplifying the controller design process. In the following subsections, we delve into the controller design for both the *reduced slow subsystem* and the *reduced fast subsystem*.

#### 3.1. Controller Design of the Reduced Slow Subsystem

Firstly, the position tracking error, denoted as  $e_1(t)$  is defined as the difference between the actual position  $q(t)$  and the desired position  $q_d(t)$ , that is,  $e_1(t) = q(t) - q_d(t)$ . Based on the given Equation (9), the error dynamics can be obtained as

$$\dot{e}_1 = e_2 \quad (13a)$$

$$\dot{e}_2 = M^{-1} \left( a u_s + (b - I) H_r \right) + W^{*T} \Phi + \zeta - \ddot{q}_d. \quad (13b)$$

To attain exceptional transient and steady-state tracking capabilities in robotic systems, it is imperative for the tracking error to remain confined within predefined boundaries, as emphasized in [8,38]

$$-\underline{\sigma} \rho(t) < e_{i1} < \bar{\sigma} \rho(t), \quad i = 1, \dots, n, \quad (14)$$

where the prescribed performance function  $\rho(t)$  can be expressed as follows:

$$\rho(t) = (\rho_0 - \rho_\infty) e^{-ht} + \rho_\infty \quad (15)$$

with  $\rho_0 \in \mathbb{R}^+$  and  $\rho_\infty \in \mathbb{R}^+$  being designed constants satisfying the condition  $0 < \rho_\infty < \rho_0$ , while  $h \in \mathbb{R}^+$  is another designed constant. Additionally,  $\underline{\sigma} \in \mathbb{R}^+$ ,  $\bar{\sigma} \in \mathbb{R}^+$  represent designed parameters.

To guarantee that the tracking error  $e_{i1}$  is bounded by the predefined boundaries, the following error transformation is first introduced [39]:

$$e_{i1}(t) = \rho S_i(\epsilon_i), \quad (16)$$

where  $\epsilon_i(t)$  represents the transformed tracking error, and the function  $S_i(\cdot)$  is given by

$$S_i(\epsilon_i) = \frac{\bar{\sigma} e^{\epsilon_i(t)} - \underline{\sigma} e^{-\epsilon_i(t)}}{e^{\epsilon_i(t)} + e^{-\epsilon_i(t)}}. \quad (17)$$

Utilizing the inverse transformation of  $S_i(\cdot)$ ,  $\epsilon_i(t)$  can be derived from (16) as:

$$\epsilon_i(t) = S_i^{-1}\left(\frac{e_{i1}(t)}{\rho(t)}\right) = \frac{1}{2} \ln \frac{\Psi_i(t) + \underline{\sigma}}{\bar{\sigma} - \Psi_i(t)}, \quad (18)$$

where  $S_i^{-1}(\bullet)$  is the inverse function of  $S_i(\epsilon_i)$ , and  $\Psi_i(t) = e_{i1}(t)/\rho(t)$  represents the intermediate variable. Let  $\epsilon = [\epsilon_1, \epsilon_2, \dots, \epsilon_n]^T$ ,  $\Psi = [\Psi_1, \Psi_2, \dots, \Psi_n]^T$ . The derivative of  $\epsilon_i$  can be derived as

$$\dot{\epsilon}_i = \frac{1}{2} z_i \dot{\Psi}_i, \quad (19)$$

where

$$z_i = \frac{1}{\Psi_i + \underline{\sigma}} - \frac{1}{\Psi_i - \bar{\sigma}}, \quad \dot{\Psi}_i = \frac{e_{i2}}{\rho} - \frac{e_{i1}\dot{\rho}}{\rho^2}, \quad \dot{\rho} = -h(\rho_0 - \rho_\infty)e^{-ht}.$$

Subsequently, the derivative of  $\dot{\epsilon}_i$  can be computed as:

$$\ddot{\epsilon}_i = \frac{1}{2} \dot{z}_i \dot{\Psi}_i + \frac{1}{2} z_i \ddot{\Psi}_i \quad (20)$$

$$= \frac{1}{2} \dot{z}_i \dot{\Psi}_i + \frac{1}{2} z_i \left( \frac{\dot{e}_{i2}}{\rho} + \frac{2e_{i1}\dot{\rho}^2}{\rho^3} - \frac{2e_{i2}\dot{\rho}}{\rho^2} - \frac{e_{i1}\ddot{\rho}}{\rho^2} \right) \quad (21)$$

$$= \frac{1}{2} \dot{z}_i \dot{\Psi}_i + \frac{1}{2} z_i \left( \frac{\dot{e}_{i2}}{\rho} + v_i \right), \quad (22)$$

where

$$\dot{z}_i = \left( \frac{1}{(\Psi_i - \bar{\sigma})^2} - \frac{1}{(\Psi_i + \underline{\sigma})^2} \right) \dot{\Psi}_i, \quad v_i = \frac{2e_{i1}\dot{\rho}^2}{\rho^3} - \frac{2e_{i2}\dot{\rho}}{\rho^2} - \frac{e_{i1}\ddot{\rho}}{\rho^2}, \quad \ddot{\rho} = h^2(\rho_0 - \rho_\infty)e^{-ht}.$$

Denote  $\Xi = \text{diag}\{z_1, z_2, \dots, z_n\}$ ,  $v = [v_1, v_2, \dots, v_n]^T$ . Then, we can respectively rewrite (19) and (21) as

$$\dot{\epsilon} = \frac{1}{2} \Xi \dot{\Psi} \quad (23a)$$

$$\ddot{\epsilon} = \frac{1}{2} \dot{\Xi} \dot{\Psi} + \frac{1}{2} \Xi \left( \frac{\dot{e}_2}{\rho} + v \right). \quad (23b)$$

Define a sliding manifold  $s_s$  as

$$s_s(t) = \dot{\epsilon}(t) - \dot{\epsilon}(0) + \int_0^t (\lambda_1^s \text{sig}(\epsilon)^{\alpha_1} + \lambda_2^s \text{sig}(\dot{\epsilon})^{\alpha_2}) d\tau, \quad (24)$$

where  $\lambda_1^s = \text{diag}\{\lambda_{11}^s, \lambda_{12}^s, \dots, \lambda_{1n}^s\}$ ,  $\lambda_2^s = \text{diag}\{\lambda_{21}^s, \lambda_{22}^s, \dots, \lambda_{2n}^s\}$  are positive definite diagonal matrices selected by the designer with  $\lambda_{ij}^s \in \mathbb{R}^+$ ,  $i = 1, 2, j = 1, \dots, n$  such that

the polynomial  $\pi^2 + \lambda_{2j}^s \pi + \lambda_{1j}^s$  is Hurwitz,  $\alpha_1 = \frac{1-\alpha_0}{1+\alpha_0}$ ,  $\alpha_2 = 1 - \alpha_0$ , with  $0 < \alpha_0 < 1$  being a positive real number,  $\text{sig}(z)^{\alpha_i} := [\text{sign}(z_1)|z_1|^{\alpha_i}, \dots, \text{sign}(z_n)|z_n|^{\alpha_i}]^T$  for a vector  $z \in \mathbb{R}^n$ ,  $i = 1, 2$ . Using (13) and (23), one has

$$\begin{aligned} \dot{s}_s &= \lambda_1^s \text{sig}(\epsilon)^{\alpha_1} + \lambda_2^s \text{sig}(\dot{\epsilon})^{\alpha_2} + \ddot{\epsilon} \\ &= \frac{\Xi}{2\rho} \left( M^{-1}(au_s + (b - I)H_r) + W^{*T}\Phi + \zeta - \ddot{q}_d + \nabla \right), \end{aligned} \quad (25)$$

where

$$\nabla = 2\rho\Xi^{-1} \left( \lambda_1^s \text{sig}(\epsilon)^{\alpha_1} + \lambda_2^s \text{sig}(\dot{\epsilon})^{\alpha_2} + \frac{1}{2}\Xi\ddot{\Psi} + \frac{\Xi}{2}\nu \right).$$

To guarantee the convergence of the sliding manifold  $s_s$ , we can design the control command  $u_s$  for the *reduced slow subsystem* as

$$u_s = a^{-1}M \left( -\hat{W}^T\Phi + \ddot{q}_d - \nabla - M^{-1}(b - I)H_r - K_1^s s_s - K_2^s \text{sig}(s_s)^{\varrho_s} - K_3^s \tanh\left(\frac{s_s}{\epsilon_s}\right) \right), \quad (26)$$

where  $K_j^s = \text{diag}\{k_{j1}^s, k_{j2}^s, \dots, k_{jn}^s\} \in \mathbb{R}^{n \times n}$ ,  $j = 1, 2, 3$  are the designed positive definite feedback gain matrix,  $\varrho_s \in \mathbb{R}^+$ ,  $\epsilon_s \in \mathbb{R}^+$  are two designed parameters satisfying  $0 < \varrho_s < 1$ ,  $0 < \epsilon_s < 1$ , and  $\hat{W} \in \mathbb{R}^{N \times n}$  is the estimation of  $W^*$ . Substituting (26) into (25), one has

$$\dot{s}_s = g_s \left( -K_1^s s_s - K_2^s \text{sig}(s_s)^{\varrho_s} - K_3^s \tanh\left(\frac{s_s}{\epsilon_s}\right) + \tilde{W}^T\Phi + \zeta \right), \quad (27)$$

where  $g_s = \frac{\Xi}{2\rho}$ ,  $\tilde{W} = W^* - \hat{W}$ .

### 3.2. Controller Design of the Reduced Fast Subsystem

Define a sliding manifold  $s_f$  for the *reduced fast subsystem* as

$$s_f(t_\epsilon) = \tau_2(t_\epsilon) - \tau_2(0) + \int_0^{t_\epsilon} (\lambda_1^f \text{sig}(\Lambda)^{\beta_1} + \lambda_2^f \text{sig}(\tau_2)^{\beta_2}) d\tau_\epsilon, \quad (28)$$

where  $\lambda_1^f = \text{diag}\{\lambda_{11}^f, \lambda_{12}^f, \dots, \lambda_{1n}^f\} \in \mathbb{R}^{n \times n}$ ,  $\lambda_2^f = \text{diag}\{\lambda_{21}^f, \lambda_{22}^f, \dots, \lambda_{2n}^f\} \in \mathbb{R}^{n \times n}$  are positive definite diagonal matrices selected by the designer with  $\lambda_{ij}^f \in \mathbb{R}^+$ ,  $i = 1, 2$ ,  $j = 1, \dots, n$  such that the polynomial  $\pi^2 + \lambda_{2j}^f \pi + \lambda_{1j}^f$  is Hurwitz,  $\beta_1 = \frac{1-\beta_0}{1+\beta_0}$ ,  $\beta_2 = 1 - \beta_0$ , with  $0 < \beta_0 < 1$  being a positive real number. The derivative of  $s_f$  with respect to  $t_\epsilon$  is

$$\frac{ds_f}{dt_\epsilon} = \lambda_1^f \text{sig}(\Lambda)^{\beta_1} + \lambda_2^f \text{sig}(\tau_2)^{\beta_2} + K_0 J^{-1} u_f - K_0 (M^{-1} + J^{-1}) \Lambda - K_0 (W^{*T}\Phi + \zeta). \quad (29)$$

To guarantee the convergence of the sliding manifold  $s_f$ , the control command  $u_f$  can be designed as

$$\begin{aligned} u_f &= J K_0^{-1} \left( -\lambda_1^f \text{sig}(\Lambda)^{\beta_1} - \lambda_2^f \text{sig}(\tau_2)^{\beta_2} + K_0 (M^{-1} + J^{-1}) \Lambda \right. \\ &\quad \left. + K_0 \hat{W}^T\Phi - K_1^f s_f - K_2^f \text{sig}(s_f)^{\varrho_f} - K_3^f \tanh\left(\frac{s_f}{\epsilon_f}\right) \right), \end{aligned} \quad (30)$$

where  $K_j^f = \text{diag}\{k_{j1}^f, k_{j2}^f, \dots, k_{jn}^f\}$ ,  $j = 1, 2, 3 \in \mathbb{R}^{n \times n}$  are the designed positive definite feedback gain matrix, and  $\varrho_f \in \mathbb{R}^+$ ,  $\epsilon_f \in \mathbb{R}^+$  are positive real numbers satisfying  $0 < \varrho_f < 1$ ,  $0 < \epsilon_f < 1$ . Substituting (30) into (29), one has

$$\frac{ds_f}{dt_\epsilon} = -K_1^f s_f - K_2^f \text{sig}(s_f)^{\varrho_f} - K_3^f \tanh\left(\frac{s_f}{\epsilon_f}\right) - K_0 (\tilde{W}^T\Phi + \zeta). \quad (31)$$



Using the controllers (26) and (30) designed for the reduced slow and fast subsystems, respectively, the overall control signal for the original high-order nonlinear FJR system (5) can be obtained as

$$u = u_s + u_f. \quad (32)$$

#### 4. Training of NN Weights

As the true nominal NN weights  $W^*$  remain unknown, in this section, we devise a composite-learning OBE-based identification algorithm to estimate  $\hat{W}$  in real time. To lay the groundwork, we present the following definition of an ellipsoid:

**Definition 1.** An  $N$ -dimensional real ellipsoid set  $\Omega$ , centered at point  $z^*$ , is mathematically represented as:

$$\Omega(z^*, F) := \{z \in \mathbb{R}^N : (z - z^*)^T F (z - z^*) \leq 1\}, \quad (33)$$

where  $F \in \mathbb{R}^{N \times N}$  denotes a positive-definite symmetric matrix.

To guarantee the boundedness of the control signal and the stability of the closed-loop system, the estimation result  $\hat{W}$  is expected to be bounded by preset compact sets  $\Omega_{c_{wi}}$  as

$$\Omega_{c_{wi}} := \{\hat{W}_i \mid \|\hat{W}_i\| < c_{wi}\}. \quad (34)$$

To facilitate the learning law design, a set of filtered variables,  $x_{2f}$ ,  $\bar{H}_f$ ,  $\Phi_f$ ,  $\bar{\tau}_{1f}$  and  $\zeta_f$  are first defined by using a first-order filter  $F_f(s) = \frac{1}{ks+1}$  ( $k > 0$ ) as

$$k\dot{x}_{2f} + x_{2f} = x_2 \quad (35a)$$

$$k\dot{\bar{H}}_f + \bar{H}_f = -M^{-1}H_r \quad (35b)$$

$$k\dot{\Phi}_f + \Phi_f = \Phi \quad (35c)$$

$$k\dot{\bar{\tau}}_{1f} + \bar{\tau}_{1f} = M^{-1}\tau_1 \quad (35d)$$

$$k\dot{\zeta}_f + \zeta_f = \zeta \quad (35e)$$

Applying the filter  $F_f(s)$  to both sides of (7b) and subsequently rearranging, we obtain

$$\psi_f(t) = \dot{x}_{2f} - \bar{H}_f - \bar{\tau}_{1f} = W^{*T}\Phi_f + \zeta_f. \quad (36)$$

Since  $\zeta$  is bounded, then the filtered optimal NN approximation error  $\zeta_f$  is also bounded; that is,  $|\zeta_{fi}| \leq \bar{\zeta}_{fi}$ , where  $\zeta_{fi}$  is the  $i$ th element of  $\zeta_f$ ,  $\bar{\zeta}_{fi} \in \mathbb{R}^+$  is a constant [40].

Employing the  $i$ th column of the matrix  $W^*$ , denoted  $W_i^*$ , from (35), we derive

$$\psi_{fi}(t) = W_i^{*T}\Phi_f + \zeta_{fi}, \quad (37)$$

where  $\psi_{fi}$  is the  $i$ th elements of  $\psi_f$ ,  $i=1$  to  $n$ . Define the identification error as

$$\tilde{\psi}_{fi} = \psi_{fi} - \hat{\psi}_{fi}, \quad (38)$$

where  $\hat{\psi}_{fi}(t) = \hat{W}_i^T\Phi_f$  is the output of the NN. Then, we propose the following composite-learning OBE algorithm to update the NN weights estimation  $\hat{W}_i$  online:

$$\dot{\hat{W}}_i = \aleph \left( \frac{\Psi_i}{\bar{\zeta}_{fi}} b_i F_i \Phi_f \tilde{\psi}_{fi} \right) + \gamma_s g_{is} F_i \Phi_f s_{is} - \gamma_f K_0 F_i \Phi_f s_{if} \quad (39a)$$

$$\dot{\tilde{F}}_i = L_i \tilde{F}_i - j_i (F_i \Phi_f \Phi_f^T F_i - F_{il} \Phi_f \Phi_f^T F_{il}) \quad (39b)$$



with

$$\varsigma_i = \frac{\lambda_i \bar{\varsigma}_{fi}^2}{1 + \Phi_f^T F_i \Phi_f} \quad (40a)$$

$$j_i = \frac{\varsigma_i L_i}{(1 - \varsigma_i) \bar{\varsigma}_{fi}^2 + \varsigma_i \Phi_f^T F_i \Phi_f} \quad (40b)$$

$$L_i = L_{i0} b_i b_p (1 - F_{iu}^{-1} \|F_i\|) \quad (40c)$$

$$\tilde{F}_i = F_i - F_{il} \quad (40d)$$

$$b_i = \begin{cases} 1, & \text{if } |\tilde{\psi}_{fi}| > \bar{\varsigma}_{fi} \text{ \& } \Phi_f^T F_i \Phi_f > \bar{\varsigma}_{fi}^2 \\ 0, & \text{if } |\tilde{\psi}_{fi}| \leq \bar{\varsigma}_{fi} \text{ or } \Phi_f^T F_i \Phi_f \leq \bar{\varsigma}_{fi}^2 \end{cases} \quad (40e)$$

for  $i = 1 \cdots n$ , let  $g_{is}$  be the  $i$ th element of  $g_s$ ,  $\lambda_i \in \mathbb{R}^+$  be a design parameter satisfying  $\lambda_i < 1/\bar{\varsigma}_{fi}^2$ , and  $o_{io} \in \mathbb{R}^+$  be a forgetting factor satisfying  $0 < o_{io} < 1$ .  $F_{il} \in \mathbb{R}^{N \times N}$  is a positive definite diagonal matrix, and  $F_{iu} \in \mathbb{R}^+$  is a positive constant that satisfies  $F_{il} < F_{iu} I$ , where  $I \in \mathbb{R}^{N \times N}$  is the identity matrix.

The projection operator, denoted by  $\aleph(\bullet)$ , is defined as follows:

$$\aleph(\bullet) = \begin{cases} \bullet, & \text{if } \|\hat{W}_i\| < c_{wi} \text{ or } \|\hat{W}_i\| = c_{wi} \text{ \& } \hat{W}_i^T \bullet \leq 0 \\ \bullet - \hat{W}_i \hat{W}_i^T \bullet / \|\hat{W}_i\|^2, & \text{otherwise} \end{cases} \quad (41)$$

and  $b_p(\bullet)$  is given by

$$b_p(\bullet) = \begin{cases} 1, & \text{if } \|\hat{W}_i\| < c_{wi} \text{ or } \|\hat{W}_i\| = c_{wi} \text{ \& } \hat{W}_i^T \bullet \leq 0 \\ 0, & \text{otherwise} \end{cases} \quad (42)$$

Define an ellipsoid set  $\Omega_{Ei}$  centered at  $W_i^*$  as

$$\Omega_{Ei}(W_i^*, F_i) = \{\hat{W}_i | \tilde{W}_i^T F_i^{-1} \tilde{W}_i \leq 1\}. \quad (43)$$

Now, we propose the following theorem.

**Theorem 1.** Consider the singularly perturbed model of an FJR (5), by using the weights updating law (39) and the NN-based adaptive controller  $u = u_s + u_f$  with  $u_s$  given in (26) and  $u_f$  given in (30), it can be guaranteed that: (1) The NN weights  $\hat{W}_i(t)$  remain inside the ellipsoid set defined in (43); that is,  $\hat{W}_i(t) \in \Omega_{Ei}, \forall t \geq 0$ . (2) The identification error  $\tilde{\psi}_{fi}$  is bounded. (3) The sliding manifolds  $s_s$  and  $s_f$  are bounded, and the tracking error  $e_1$  is bounded by the predefined performance boundaries.

A detailed proof of Theorem 1 is presented in Appendix A.

**Remark 2.** In this study, we propose an adaptive PPC tailored for FJR. Departing from conventional approaches that employ back-stepping or dynamic surface control methodologies [6–9], our design leverages the SPT to reduce system complexity and simplify the controller synthesis process, thereby significantly enhancing its practical applicability to actual FJR systems. Furthermore, unlike other research efforts [10,11] that solely rely on SMC or PPC to counteract disturbances, this work introduces an online-trained NN to approximate and mitigate unknown perturbations, significantly enhancing control precision. This innovative utilization of SPT, PPC and NNs constitutes the first key contribution of our paper.

**Remark 3.** This paper presents a novel composite-learning OBE algorithm for online updating of NN weights. Diverging from conventional OBE methods in the literature [13,32–34], which solely utilize identification error, our approach uniquely integrates tracking errors from both the slow

and fast subsystems into the weight updating process. This innovative strategy yields substantial enhancements in identification and tracking precision, constituting the second major contribution of this study.

## 5. Simulation Study

In this section, Matlab simulations of a two-degrees-of-freedom FJR are reported to verify the effectiveness of the identification and control algorithm proposed in this study. The schematic diagram of the  $i$ th link of the FJR is depicted in Figure 1. The matrices  $\mathbf{M}(q)$ ,  $\mathbf{C}(q, \dot{q})$ ,  $\mathbf{G}(q)$  of the FJR model (1) are given by

$$\begin{aligned} \mathbf{M}(q) &= \begin{bmatrix} M_{11} & M_{12} \\ M_{21} & M_{22} \end{bmatrix}, \quad \mathbf{C}(q, \dot{q}) = \begin{bmatrix} C_1 \\ C_2 \end{bmatrix}, \quad \mathbf{G}(q) = \begin{bmatrix} G_1 \\ G_2 \end{bmatrix}, \\ M_{11} &= m_1 l_{c1}^2 + I_1 + I_2 + m_2 (l_1^2 + l_{c2}^2 + 2l_1 l_{c2} \cos q_2), \\ M_{12} &= m_2 l_{c2}^2 + I_2 + m_2 l_2 l_{c2} \cos q_2 \\ M_{21} &= m_2 l_{c2}^2 + I_2 + m_2 l_2 l_{c2} \cos q_2, \quad M_{22} = m_2 l_{c2}^2 + I_2 \\ C_1 &= -m_2 l_1 l_{c2} \sin q_2 \dot{q}_2 - m_2 l_1 l_{c2} \sin q_2 (\dot{q}_1 + \dot{q}_2), \quad C_2 = m_2 l_1 l_{c2} \sin q_2 \dot{q}_1 \\ G_1 &= m_2 g l_1 \cos(q_1 + q_2) + (m_1 + m_2) g l_1 \cos q_1, \quad G_2 = m_2 g l_2 \cos(q_1 + q_2) \end{aligned}$$

and the nominal system parameters used in the simulation are listed in Table 1. For simplicity, no friction is considered in the simulation; thus,  $D = [0, 0]^T$ . To verify the effectiveness of the proposed methods for systems with model uncertainties, the real system parameters  $m_1^*$ ,  $m_2^*$ ,  $I_1^*$ ,  $I_2^*$ ,  $l_1^*$ ,  $l_2^*$ ,  $l_{c1}^*$ ,  $l_{c2}^*$  are set to be 1.2 times of their nominal values. The reference signal is  $q_d = [\sin(1.6\pi t), \sin(1.6\pi t + \pi/3)]^T$ . The initial values for  $x_1$  and  $x_2$  are  $x_1(0) = 0.8$  and  $x_2(0) = 0$ . To transform the original system model (1) into a singular perturbation model (2),  $K_0 = \text{diag}\{0.01, 0.01\}$  is used. The prescribed performance continuous terminal sliding mode controller based on the singular perturbation technique and the composite-learning optimal bounded ellipsoid algorithm (SOBE) is used to control this system, and the following parameters are chosen for the controller:  $K_1^s = 5$ ,  $K_2^s = 1$ ,  $K_3^s = 1$ ,  $\epsilon_s = 0.1$ ,  $\rho_s = 0.9$ ,  $K_1^f = 250$ ,  $K_2^f = 1$ ,  $K_3^f = 1$ ,  $\epsilon_f = 0.1$ ,  $\rho_f = 0.9$ . To compensate the uncertainties, an NN with 30 neurons is employed, and the identification algorithm parameters are chosen as:  $\gamma_s = 0.02$ ,  $\gamma_f = 0.02$ ,  $L_{i0} = 0.2$ ,  $F_{il} = 20I$ ,  $F_{iu} = 200$ ,  $\lambda_i = 5$ ,  $\bar{\zeta}_{fi} = 0.001$ .

**Table 1.** Nominal parameters of the manipulator.

Parameter	Value	Unit
$m_1, m_2$	0.1	kg
$l_1, l_2$	0.4	m
$I_1, I_2$	0.02	kg·m <sup>2</sup>
$l_{c1}, l_{c2}$	0.2	m
$J_1, J_2$	0.01	kg·m <sup>2</sup>
K	9	N·m/rad

For the purpose of comparison, a modified OBE algorithm (MOBE)-based adaptive controller [13] is also tested in the simulation. The choice of this particular control scheme is motivated by the fact that our identification methodology builds upon the MOBE framework. While MOBE exclusively utilizes the identification error for updating NN weights, our proposed method incorporates both identification and tracking errors in the NN training process, thereby extending the MOBE approach. Additionally, whereas [13] employs a conventional sliding mode controller, our study develops a terminal sliding mode PPC. Consequently, [13] constitutes an apt and informative reference point against which to assess the performance of our novel controller. For the MOBE method, all the shared parameters are the same as those used for SOBE. It should be pointed out that the control

method proposed in [13] is only used to control the reduced slow subsystem. The controller for the reduced fast subsystem is the same as the one used in SOBE.

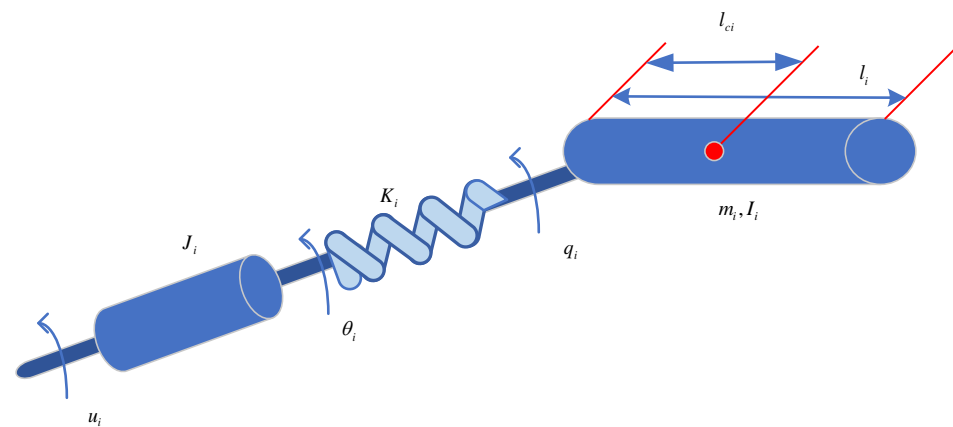


**Figure 1.** Schematic diagram of link  $i$  of the FJR. In the diagram,  $m_i$ ,  $I_i$  are the mass and moment of inertia of the link  $i$ ,  $l_i$  is the length of the link  $i$ , and  $l_{ci}$  denotes the position of the center of mass of link  $i$ ,  $i = 1, 2$ .

The simulation outcomes are presented in Figures 2–17. As is evident from Figures 2 and 3, both the SOBE and MOBE methods enable the system state  $x_1$  to track the designated reference  $x_r$ . However, the angular position of the robot converges faster to the reference when employing the SOBE controller, resulting in smaller disparities between the system state and the reference signal.

Additionally, Figures 4 and 5 clearly illustrate that the SOBE method yields smaller position tracking errors, which converge to 0 more rapidly. Notably, the predefined performance boundaries are consistently upheld throughout the entire identification and control process. Conversely, the MOBE method exhibits a larger tracking error and a slower convergence rate.

Furthermore, Figures 6 and 7 demonstrate that when using the SOBE method, the angular velocity rapidly approaches its reference signal  $\dot{x}_r$  and maintains close alignment thereafter. In contrast, the MOBE method leads to slower convergence and larger disparities. Similarly, Figures 8 and 9 show that the SOBE method achieves reduced velocity tracking errors, which converge to a small residual set centered around 0 more quickly.

It is worth mentioning that since both the SOBE and MOBE methods employ the same controller for the reduced fast controller,  $\tau_1$  tracks  $h(x)$  well regardless of the method used, as depicted in Figures 10 and 11.

The identification results are presented in Figures 12 and 13, while the identification errors are depicted in Figures 14 and 15. Both figures reveal that the integration of tracking error into the learning law enhances the performance of the composite-learning OBE algorithm. Specifically, the estimation results  $\hat{\psi}_{fi}$  converge to  $\psi_{fi}$  more rapidly. Conversely, when the MOBE algorithm is employed, the estimation results take longer to converge to the true values.

It is noteworthy that in Figures 14 and 15, the steady-state NN identification errors associated with the MOBE exhibit smaller magnitudes. This observation can be attributed to the fact that, in the MOBE framework, only the identification error  $\tilde{\psi}_{fi}$  serves as the basis for updating NN weights, with the aim of having  $\hat{\psi}_{fi} = \hat{W}_i^T \Phi_f$  closely approximate  $\psi_{fi}$ . By contrast, the SOBE approach introduces tracking errors from the reduced subsystems into the weight updating mechanism. Consequently, the NN not only strives to approximate  $\psi_{fi}$  but also compensates for model discrepancies arising from the SPT-induced order reduction, ultimately minimizing tracking errors. Thus, while the discrepancy between  $\hat{W}_i^T \Phi_f$  and  $\psi_{fi}$  may be larger when employing the SOBE method, the associated tracking errors are concurrently smaller.

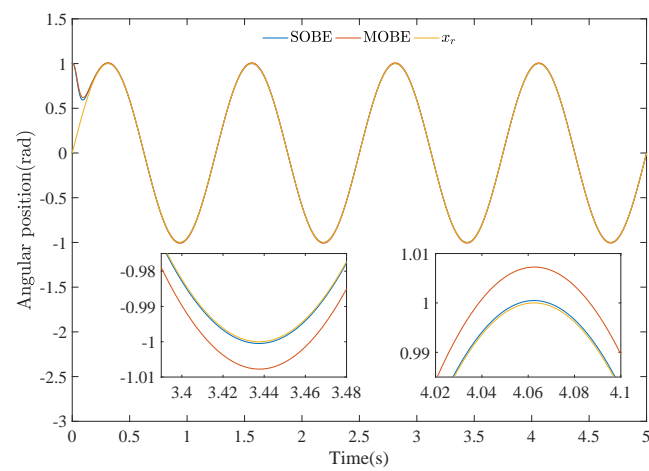


Figure 2. Angular position for joint 1.

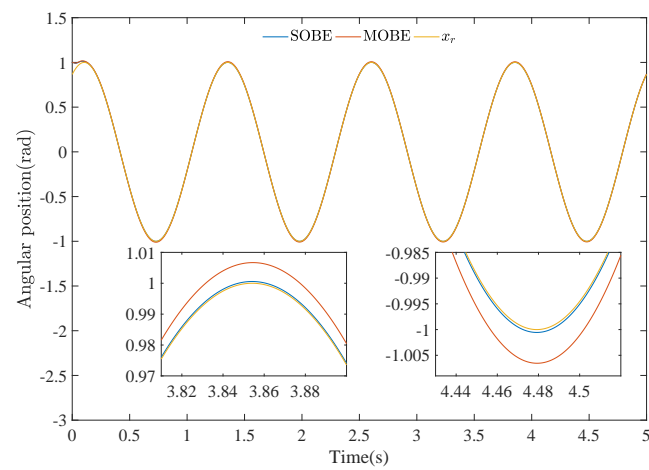


Figure 3. Angular position for joint 2.

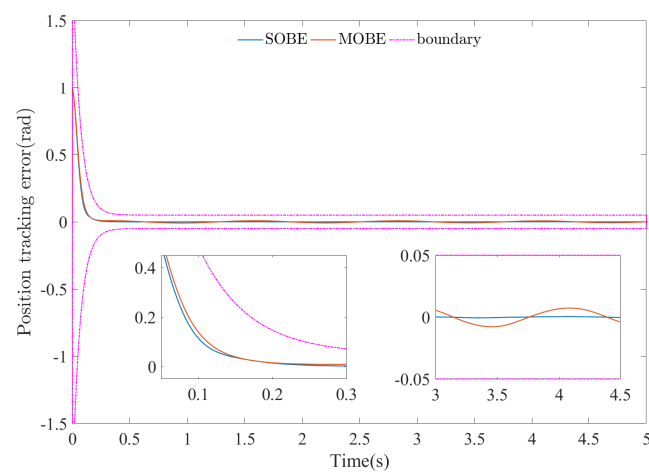


Figure 4. Angular position error for joint 1.

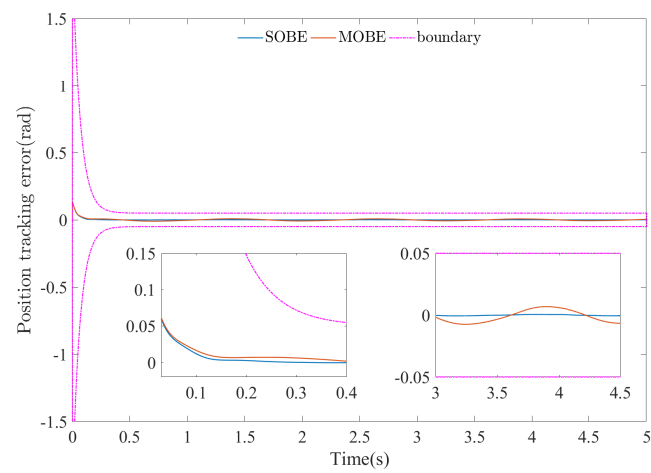


Figure 5. Angular position error for joint 2.

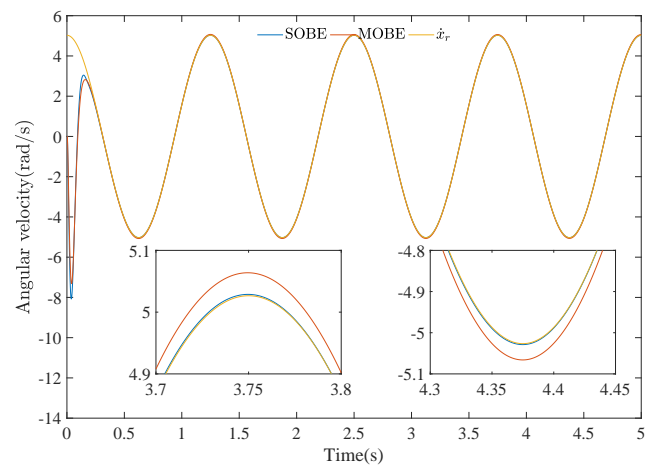


Figure 6. Angular velocity for joint 1.

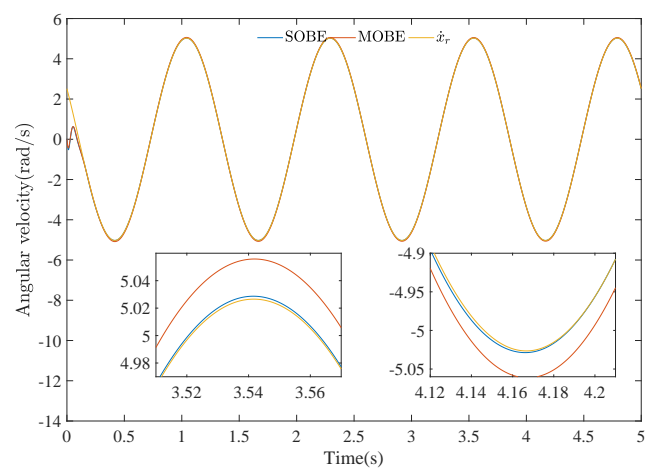
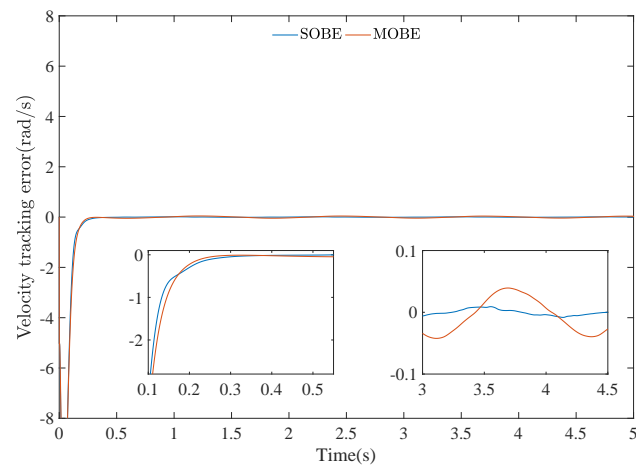
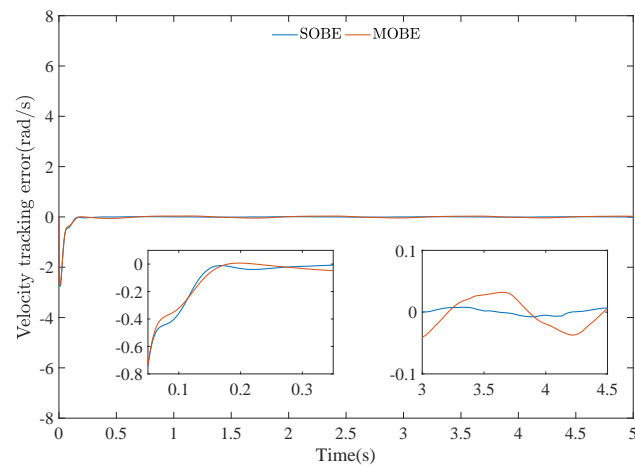


Figure 7. Angular velocity for joint 2.



**Figure 8.** Velocity tracking error for joint 1.



**Figure 9.** Velocity tracking error for joint 2.

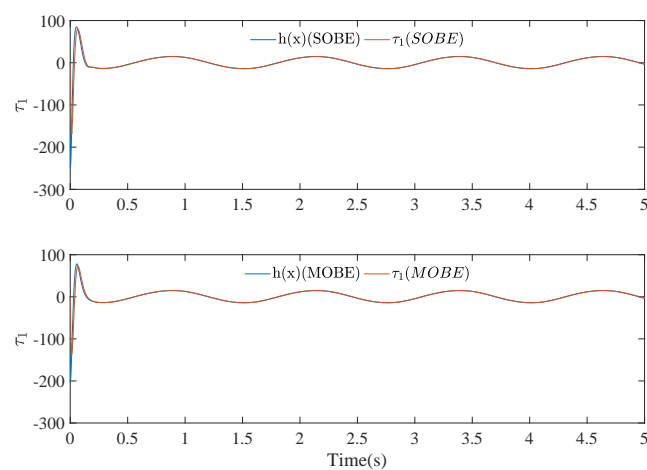


**Figure 10.** Tracking results of  $\tau_1$  for joint 1.

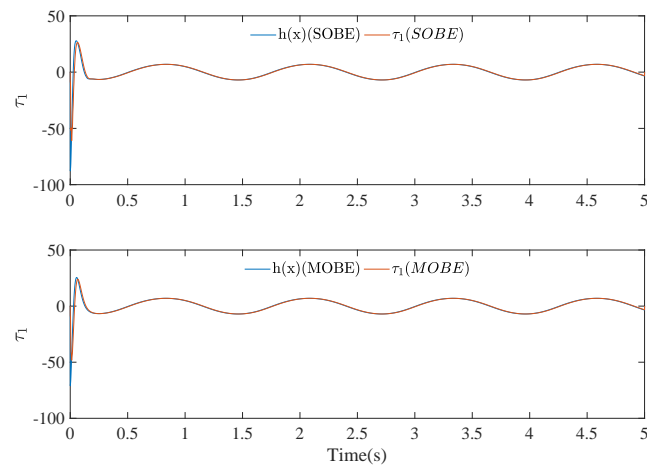


Figure 11. Tracking results of  $\tau_1$  for joint 2.

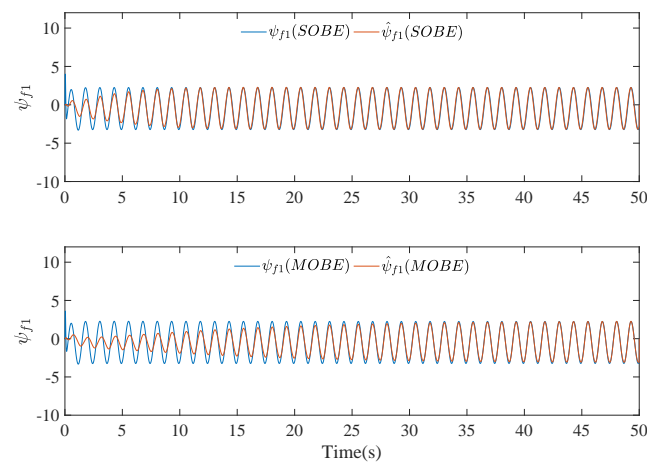


Figure 12. NN estimation results for joint 1.

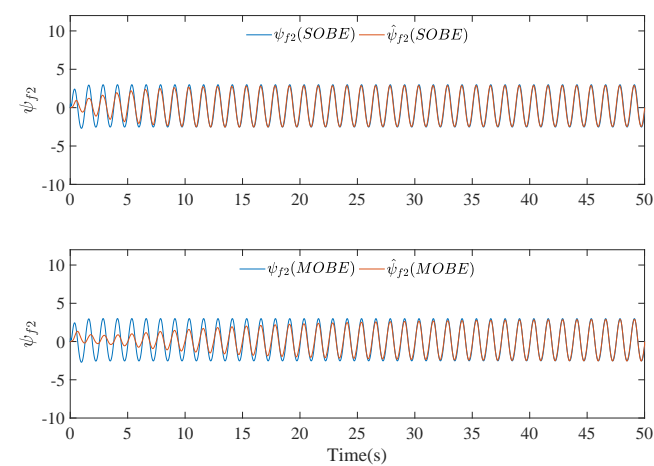


Figure 13. NN estimation results for joint 2.



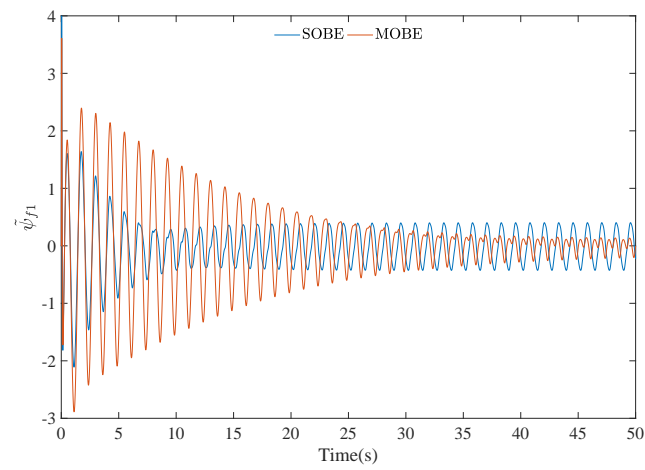


Figure 14. NN estimation errors for joint 1.

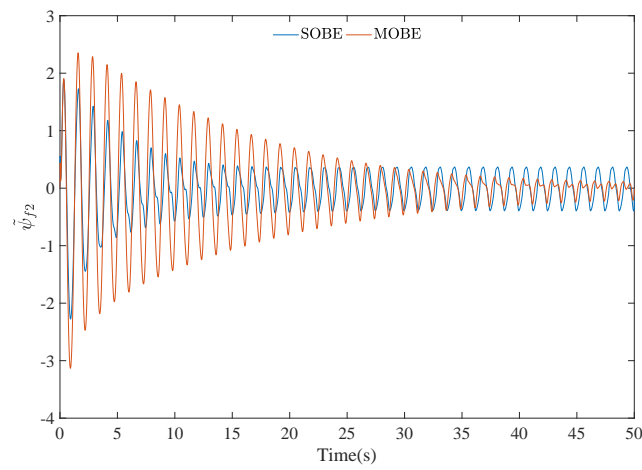


Figure 15. NN estimation errors for joint 2.

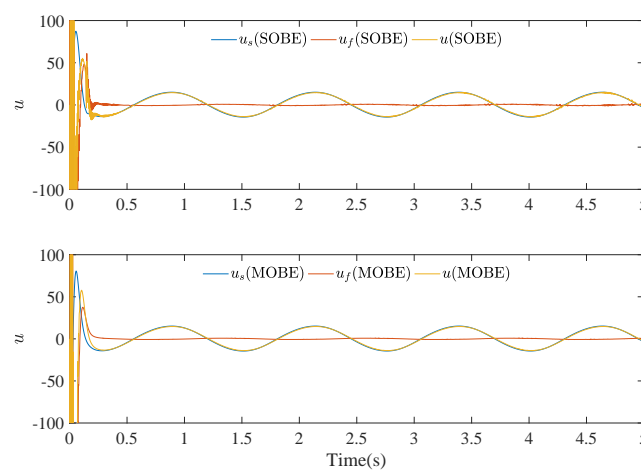


Figure 16. Control signal for joint 1.

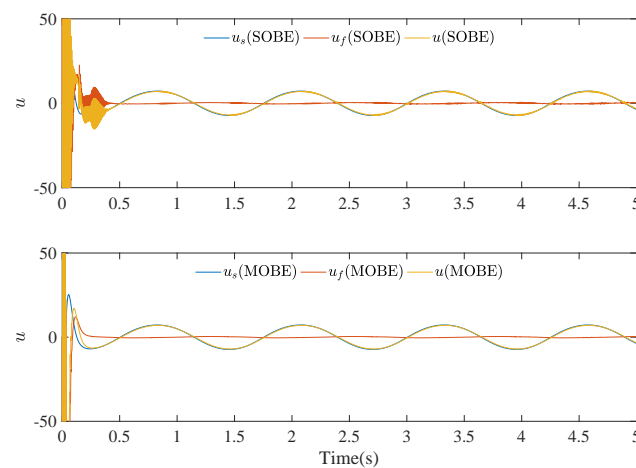


Figure 17. Control signal for joint 2.

The control signals generated by both the SOBE and MOBE methodologies are illustrated in Figures 16 and 17. Evidently, during the transient phase, the amplitude of  $u_f$  is substantial, facilitating the swift convergence of the fast state  $\tau_1$  to its equilibrium value  $h(x, t)$ . Subsequently,  $u_f$  diminishes to near-zero levels at steady state. This characteristic response exemplifies the inherent behavior of a singularly perturbed system.

The figures presented in this study demonstrate that the SOBE method, which incorporates tracking errors into the NN weight updating law and utilizes the PPC to constrain error boundaries, significantly outperforms the MOBE method. Specifically, the SOBE method exhibits superior identification and control performance, as compared to the MOBE method, which relies solely on a regular sliding mode control approach and updates NN weights based solely on identification errors.

## 6. Conclusions

This paper introduces a novel identification and adaptive control algorithm tailored for FJR, aimed at enhancing NN training efficiency and trajectory tracking accuracy. We begin by applying the SPT method to decompose the intricate high-order system into two easily-managed low-order subsystems. This simplifies controller design by focusing on these reduced-order components instead of the full high-order system. To ensure desired transient and steady-state characteristics, we integrate the PPC technique into the slow subsystem's controller design. For faster convergence, continuous terminal sliding mode controllers are developed for both slow and fast subsystems. Additionally, we boost identification performance by merging the tracking error with the conventional OBE algorithm, creating a novel composite-learning OBE-based learning rule.

Simulations reveal that using the proposed identification and control algorithm leads to closer tracking of reference states, quicker convergence of tracking errors to zero, and smaller steady-state tracking errors. This improved performance is attributed to the capture of model uncertainties resulting from system order reduction, as tracking errors are also utilized to train NN weights. Furthermore, NN training speed is accelerated.

The immediate next step involves implementing the proposed algorithm on a real multi-link FJR to further validate its practical efficacy. Given that many practical FJR systems experience input saturation nonlinearity due to limited motor drive capacity, investigating SPT-based PPC under input saturation constraints is warranted. Lastly, while this paper establishes the closed-loop system's boundedness, proving its finite-time convergence would be a valuable future extension.

**Author Contributions:** Conceptualization, D.Z. and X.R.; methodology, D.Z. and K.G.; software, X.L. and D.Z.; validation, D.Z., K.G. and X.R.; formal analysis, X.L., D.Z. and X.R.; investigation, X.L. and D.Z.; resources, K.G. and X.R.; data curation, X.L. and D.Z.; writing—original draft preparation, X.L.; writing—review and editing, D.Z., K.G. and X.R.; visualization, X.L.; supervision, D.Z.; project administration, X.R.; funding acquisition, D.Z. and K.G. All authors have read and agreed to the published version of the manuscript.

**Funding:** This work is supported in part by the National Nature Science Foundation under Grant No. 62103051, 52205035, in part by the the National Key R&D Program of China under Grant No. 2023YFB4703900, and in part by the Beijing Institute of Technology Research Fund Program for Young Scholars.

**Institutional Review Board Statement:** Not applicable.

**Informed Consent Statement:** Not applicable.

**Data Availability Statement:** The data presented in this study are available on request from the corresponding author due to privacy.

**Conflicts of Interest:** The authors declare no conflicts of interest.

## Notations

The following notations are used in this manuscript:

$q, \dot{q}$	angular position and velocity of the joint
$\theta, \dot{\theta}$	angular position and velocity of the motor
$M(q)$	the inertia matrix
$C(q, \dot{q})$	the centripetal/Coriolis matrix
$D(\dot{q})$	the friction torque vector
$G(q)$	the gravity torque vector
$\tau_d$	the aggregate disturbance
$u, u_s, u_f$	the system input vector, control command of the reduced slow subsystem and control command of the reduced fast subsystem
$K$	the stiffness matrix of the spring between the motor and the link
$J$	the inertia matrix of the motors
$x_1, x_2$	$q$ and $\dot{q}$
$\tau_1, \tau_2$	the elastic torque and its derivative with respect to $t_\varepsilon$
$h(x, t)$	the equilibrium of $\tau_1$
$\Lambda$	the difference between $\tau_1$ and $h(x, t)$
$W^*, \Phi$	the NN weight matrix and regression functions vector
$N$	the number of neurons used in the hidden layer
$\zeta$	the NN approximation error
$t_\varepsilon$	the fast time scale
$e_1, e_2$	the position tracking error and the velocity tracking error
$\rho(t)$	the prescribed performance function
$\varepsilon_i(t)$	the transformed tracking error of $e_{1i}$
$s_s, s_f$	the slow sliding manifold and the fast sliding manifold
$K_1^s, K_2^s, K_3^s$	the feedback gain matrices of $u_s$
$K_1^f, K_2^f, K_3^f$	the feedback gain matrices of $u_f$
$\Omega_{c_{wi}}$	preset compact sets for $\hat{W}_i$
$\Omega_{Ei}$	the ellipsoid set of $\tilde{W}_i$
$x_{2f}, \tilde{H}_f, \Phi_f, \bar{\tau}_{1f}$ and $\zeta_f$	filtered results of $x_2, -M^{-1}H_r, \Phi, M^{-1}\tau_1$ and $\zeta$
$F_i$	the learning gain matrix of the NN weight's updating law
$\hat{\psi}_{fi}$	the filtered output of the NN

## Appendix A. Proof of Theorem 1

**Proof.** To facilitate the stability analysis, several basic lemmas and definitions are given first.

**Lemma A1.** [13] By using the updating law (39b), it can be guaranteed that the learning gain  $F_i(t)$  has deterministic and predeterminable bounds, that is,  $F_{il} < F_i(t) \leq F_{iu}I, \forall t \geq 0$ .

**Lemma A2.** [41] The following inequality holds for any  $\epsilon_0 > 0$  and  $x_0 \in \mathbb{R}$ :

$$0 \leq |x_0| - x_0 \tanh\left(\frac{x_0}{\epsilon_0}\right) \leq \kappa_0 \epsilon_0, \quad (\text{A1})$$

where  $\kappa_0$  is a constant satisfying  $\kappa_0 = e^{-(\kappa_0+1)}$ , i.e.,  $\kappa_0 = 0.2785$ .

The proof of Theorem 1 comprises the following steps:

**Step 1,** the boundedness of the NN weights  $\hat{W}_i$  are proved.

Choose a Lyapunov function candidate

$$V_{oi} = \gamma_s s_{is}^2 + \tilde{W}_i^T F_i^{-1} \tilde{W}_i + \epsilon \gamma_f s_{if}^2, \quad (\text{A2})$$

where  $s_{is}$  and  $s_{if}$  are the  $i$ th elements of  $s_s$  and  $s_f$ , respectively. The time derivative of  $V_{oi}$  is given as

$$\dot{V}_{oi} = 2\gamma_s s_{is} \dot{s}_{is} - 2\tilde{W}_i^T F_i^{-1} \dot{\tilde{W}}_i + \tilde{W}_i^T F_i^{-1} \tilde{W}_i + \frac{2\gamma_f s_{if} ds_{if}}{dt_\epsilon}. \quad (\text{A3})$$

Noting the result of the projection operation, if  $\hat{W}_i(0) \in \Omega_{c_{wi}}$ , then the parameter learning law ensures  $\hat{W}_i(t) \in \Omega_{c_{wi}}$  and

$$\tilde{W}_i^T F_i^{-1} \dot{\tilde{W}}_i \geq \tilde{W}_i^T F_i^{-1} \left( \frac{\zeta_i}{\bar{\zeta}_{fi}^2} b_i F_i \Phi_f \tilde{\psi}_{fi} + \gamma_s g_{is} F_i \Phi s_{is} - \gamma_f K_0 F_i \Phi s_{if} \right). \quad (\text{A4})$$

Applying the foregoing inequality to (A3), one obtains

$$\begin{aligned} \dot{V}_{oi} \leq & -2 \frac{\zeta_i}{\bar{\zeta}_{fi}^2} b_i \tilde{W}_i^T \Phi_f \tilde{\psi}_{fi} - 2\gamma_s g_{is} F_i \tilde{W}_i^T F_i^{-1} \Phi s_{is} + 2\gamma_f K_0 F_i \tilde{W}_i^T F_i^{-1} \Phi s_{if} \\ & + 2\gamma_s s_{is} \dot{s}_{is} + \tilde{W}_i^T F_i^{-1} \tilde{W}_i + \frac{2\gamma_f s_{if} ds_{if}}{dt_\epsilon}. \end{aligned} \quad (\text{A5})$$

**Case 1a:** When  $|\tilde{\psi}_{fi}| > \bar{\zeta}_{fi}$  &  $\Phi_f^T F_i \Phi_f > \bar{\zeta}_{fi}^2$  hold, and  $\|\hat{W}_i\| < c_{wi}$  or  $\|\hat{W}_i\| = c_{wi}$  &  $\hat{W}_i^T \bullet \leq 0$  hold, that is,  $b_i = 1$  and  $b_p = 1$  in this case. Combining (A5) and (39a), one obtains

$$\begin{aligned}
\dot{V}_{oi} &\leq -\frac{\zeta_i}{\bar{\zeta}_{fi}^2} \tilde{W}_i^T \Phi_f (\tilde{W}_i^T \Phi_f + \zeta_{fi}) - \frac{\zeta_i}{\bar{\zeta}_{fi}^2} (\tilde{\psi}_{fi} - \zeta_{fi}) \tilde{\psi}_{fi} \\
&\quad - 2\gamma_s g_{is} F_i \tilde{W}_i^T F_i^{-1} \Phi s_{is} + 2\gamma_f K_0 F_i \tilde{W}_i^T F_i^{-1} \Phi s_{if} - L_i \tilde{W}_i^T F_i^{-1} F_i F_i^{-1} \tilde{W}_i \\
&\quad + j_i \tilde{W}_i^T F_i^{-1} (F_i \Phi_f \Phi_f^T F_i - F_{il} \Phi_f \Phi_f^T F_{il}) F_i^{-1} \tilde{W}_i \\
&\quad + 2\gamma_s s_{is} g_{is} \left( -k_{1i}^s s_{is} - k_{2i}^s \text{sig}(s_{is})^{q_s} - k_{3i}^s \tanh\left(\frac{s_{is}}{\epsilon_s}\right) + \tilde{W}_i^T \Phi + \zeta_i \right) \\
&\quad + 2\gamma_f s_{if} \left( -k_{1i}^f s_{if} - k_{2i}^f \text{sig}(s_{if})^{q_f} - k_{3i}^f \tanh\left(\frac{s_{if}}{\epsilon_f}\right) - K_0 (\tilde{W}_i^T \Phi + \zeta_i) \right) \\
&\leq -\left(\frac{\zeta_i}{\bar{\zeta}_{fi}^2} - j_i\right) \tilde{W}_i^T \Phi_f \Phi_f^T \tilde{W}_i - \frac{\zeta_i}{\bar{\zeta}_{fi}^2} (\tilde{\psi}_{fi}^2 - \zeta_{fi}^2) \\
&\quad + 2\gamma_s s_{is} g_{is} \left( -k_{1i}^s s_{is} - k_{2i}^s \text{sig}(s_{is})^{q_s} - k_{3i}^s \tanh\left(\frac{s_{is}}{\epsilon_s}\right) + \zeta_i \right) \\
&\quad + 2\gamma_f s_{if} \left( -k_{1i}^f s_{if} - k_{2i}^f \text{sig}(s_{if})^{q_f} - k_{3i}^f \tanh\left(\frac{s_{if}}{\epsilon_f}\right) - K_0 \zeta_i \right). \tag{A6}
\end{aligned}$$

Using Lemma A2, the above equation can be further rewritten as:

$$\begin{aligned}
&\leq -\|\Phi_f\|^2 \left( \frac{\zeta_i}{\bar{\zeta}_{fi}^2} - j_i \right) \|\tilde{W}_i\|^2 - \frac{\zeta_i}{\bar{\zeta}_{fi}^2} (\tilde{\psi}_{fi}^2 - \zeta_{fi}^2) - 2\gamma_s g_{is} k_{1i}^s |s_{is}|^2 - 2\gamma_s g_{is} k_{2i}^s |s_{is}|^{1+q_s} \\
&\quad - 2\gamma_f k_{1i}^f |s_{if}|^2 - 2\gamma_f k_{2i}^f |s_{if}|^{1+q_f} - (-2\gamma_s g_{is} |\zeta_i| + 2\gamma_s g_{is} k_{3i}^s) |s_{is}| \\
&\quad - (2\gamma_f k_{3i}^f + 2K_0 \gamma_f |\zeta_i|) |s_{if}| + 2\gamma_s g_{is} k_{3i}^s \kappa_0 \epsilon_s + 2\gamma_f k_{3i}^f \kappa_0 \epsilon_f \\
&\leq -\|\Phi_f\|^2 \left( \frac{\zeta_i}{\bar{\zeta}_{fi}^2} - j_i \right) \|\tilde{W}_i\|^2 - 2\gamma_s g_{is} k_{1i}^s |s_{is}|^2 - 2\gamma_f k_{1i}^f |s_{if}|^2 + 2\gamma_s g_{is} k_{3i}^s \kappa_0 \epsilon_s + 2\gamma_f k_{3i}^f \kappa_0 \epsilon_f \\
&\leq -\alpha_{v1i} V_{oi} + \beta_{v1i}, \tag{A7}
\end{aligned}$$

where  $\alpha_{v1i} = \min\{\|\Phi_f\|^2(\frac{\zeta_i}{\bar{\zeta}_{fi}^2} - j_i), 2\gamma_s g_{is} k_{1i}^s, 2\gamma_f k_{1i}^f\}$ ,  $\beta_{v1i} = 2\gamma_s g_{is} k_{3i}^s \kappa_0 \epsilon_s + 2\gamma_f k_{3i}^f \kappa_0 \epsilon_f$ .

From  $0 < \zeta_i < 1$  and  $\phi_f^T F_i \phi_f > \bar{\zeta}_{fi}^2$ , one obtains  $(1 - \zeta_i)\bar{\zeta}_{fi}^2 + \zeta_i \phi_f^T F_i \phi_f > \bar{\zeta}_{fi}^2$ . Noting  $0 < L_{i0} < 1$ , it can be obtained  $(\zeta_i/\bar{\zeta}_{fi}^2) - j_i > 0$ . It is clear that  $\dot{V}_{oi} < 0$  is true as long as  $V > \frac{\beta_{v1i}}{\alpha_{v1i}}$ .

Case 1b: When  $|\tilde{\psi}_{fi}| > \bar{\zeta}_{fi}$  &  $\Phi_f^T F_i \Phi_f > \bar{\zeta}_{fi}^2$  hold, and  $\|\hat{W}_i\| > c_{wi}$  or  $\|\hat{W}_i\| = c_{wi}$  &  $\hat{W}_i^T \bullet > 0$  hold, that is,  $b_i = 1$  and  $b_p = 0$  in this case, which implies  $\dot{F}_i = 0$ . Combining (A5) and (39a), it yields:

$$\begin{aligned}
\dot{V}_{oi} &\leq -\frac{\zeta_i}{\bar{\zeta}_{fi}^2} \tilde{W}_i^T \Phi_f (\tilde{W}_i^T \Phi_f + \zeta_{fi}) - \frac{\zeta_i}{\bar{\zeta}_{fi}^2} (\tilde{\psi}_{fi} - \zeta_{fi}) \tilde{\psi}_{fi} \\
&\quad - 2\gamma_s g_{is} F_i \tilde{W}_i^T F_i^{-1} \Phi s_{is} + 2\gamma_f K_0 F_i \tilde{W}_i^T F_i^{-1} \Phi s_{if} \\
&\quad + 2\gamma_s s_{is} g_{is} \left( -k_{1i}^s s_{is} - k_{2i}^s \text{sig}(s_{is})^{q_s} - k_{3i}^s \tanh\left(\frac{s_{is}}{\epsilon_s}\right) + \tilde{W}_i^T \Phi + \zeta_i \right) \\
&\quad + 2\gamma_f s_{if} \left( -k_{1i}^f s_{if} - k_{2i}^f \text{sig}(s_{if})^{q_f} - k_{3i}^f \tanh\left(\frac{s_{if}}{\epsilon_f}\right) - K_0 (\tilde{W}_i^T \Phi + \zeta_i) \right) \\
&\leq -\|\Phi_f\|^2 \frac{\zeta_i}{\bar{\zeta}_{fi}^2} \|\tilde{W}_i\|^2 - \frac{\zeta_i}{\bar{\zeta}_{fi}^2} (\tilde{\psi}_{fi}^2 - \zeta_{fi}^2) - 2\gamma_s g_{is} k_{1i}^s |s_{is}|^2 \\
&\quad - 2\gamma_f k_{1i}^f |s_{if}|^2 + 2\gamma_s g_{is} k_{3i}^s \kappa_0 \epsilon_s + 2\gamma_f k_{3i}^f \kappa_0 \epsilon_f \\
&\leq -\alpha_{v2i} V_{oi} + \beta_{v2i},
\end{aligned} \tag{A8}$$

where  $\alpha_{v2i} = \min\{\|\Phi_f\|^2 \frac{\zeta_i}{\bar{\zeta}_{fi}^2}, 2\gamma_s g_{is} k_{1i}^s, 2\gamma_f k_{1i}^f\}$ ,  $\beta_{v2i} = 2\gamma_s g_{is} k_{3i}^s \kappa_0 \epsilon_s + 2\gamma_f k_{3i}^f \kappa_0 \epsilon_f$ . Noting  $|\tilde{\psi}_{fi}| > \bar{\zeta}_{fi}$ ,  $\bar{\zeta}_{fi} \geq |\zeta_{fi}|$ . It is clear that  $\dot{V}_{oi} < 0$  is true as long as  $V > \frac{\beta_{v2i}}{\alpha_{v2i}}$ .

Case 1c: When  $|\tilde{\psi}_{fi}| \leq \bar{\zeta}_{fi}$  &  $\Phi_f^T F_i \Phi_f \leq \bar{\zeta}_{fi}^2$  hold, that is,  $b_i = 0$  in this case, which implies  $\tilde{F}_i = 0$ . Combining (A5) and (39a), one obtains:

$$\begin{aligned}
\dot{V}_{oi} &\leq -2\gamma_s g_{is} F_i \tilde{W}_i^T F_i^{-1} \Phi s_{is} + 2\gamma_f K_0 F_i \tilde{W}_i^T F_i^{-1} \Phi s_{if} \\
&\quad + 2\gamma_s s_{is} g_{is} \left( -k_{1i}^s s_{is} - k_{2i}^s \text{sig}(s_{is})^{q_s} - k_{3i}^s \tanh\left(\frac{s_{is}}{\epsilon_s}\right) + \tilde{W}_i^T \Phi + \zeta_i \right) \\
&\quad + 2\gamma_f s_{if} \left( -k_{1i}^f s_{if} - k_{2i}^f \text{sig}(s_{if})^{q_f} - k_{3i}^f \tanh\left(\frac{s_{if}}{\epsilon_f}\right) - K_0 (\tilde{W}_i^T \Phi + \zeta_i) \right) \\
&\leq -2\gamma_s g_{is} k_{1i}^s |s_{is}|^2 - 2\gamma_f k_{1i}^f |s_{if}|^2 + 2\gamma_s g_{is} k_{3i}^s \kappa_0 \epsilon_s + 2\gamma_f k_{3i}^f \kappa_0 \epsilon_f \\
&\leq -\alpha_{v3i} V_{oi} + \beta_{v3i},
\end{aligned} \tag{A9}$$

where  $\alpha_{v3i} = \min\{2\gamma_s g_{is} k_{1i}^s, 2\gamma_f k_{1i}^f\}$ ,  $\beta_{v3i} = 2\gamma_s g_{is} k_{3i}^s \kappa_0 \epsilon_s + 2\gamma_f k_{3i}^f \kappa_0 \epsilon_f$ . It is clear that  $\dot{V}_{oi} < 0$  is true as long as  $V > \frac{\beta_{v3i}}{\alpha_{v3i}}$ .

Combining the above analysis in cases 1a-1c, it can be concluded that  $\hat{W}_i(t) \in \Omega_{E_i}, \forall t \geq 0$  if  $\hat{W}_i(0) \in \Omega_{E_i}$ .

**Step 2**, the boundedness of the identification error  $\tilde{\psi}_{fi}$  is proved.

Since  $\hat{W}_i(t) \in \Omega_{E_i}$  holds, it can be obtained that  $\tilde{W}_i(t)$  remain in the ellipsoid set defined (43), that is

$$\tilde{W}_i^T F_{iu} \tilde{W}_i \leq \tilde{W}_i^T F_i^T \tilde{W}_i \leq 1. \tag{A10}$$

Therefore, one obtains

$$\|\tilde{W}_i\| \leq \sqrt{F_{iu}}. \tag{A11}$$

Moreover,  $\Phi$  is bounded  $\forall e \in \Omega_{ce}$ , that is,  $\|\Phi_f\| \leq \bar{\phi}$ , where  $\bar{\phi} \in R^+$  is a constant. Therefore, it can be obtained that  $\|\tilde{\psi}_{fi}\| = \|\tilde{W}_i^T \Phi_f\| \leq \sqrt{F_{iu}} \bar{\phi}$ .

**Step 3**, the boundedness of the tracking errors is proved.

Since the Lyapunov function candidate  $V_{oi}$  is bounded, it can be further inferred that  $s_s, s_f$  also converges to a small residual set around 0, which also means the tracking error  $e_1$  of the *reduced slow subsystem* is bounded by the predefined performance boundaries and converges to a small residual set around 0. Since the stability of both subsystems is

guaranteed, then, according to Tikhonov's theorem, the stability of the original high-order system is also guaranteed.  $\square$

## References

- Iskandar, M.; van Ommeren, C.; Wu, X.; Albu-Schäffer, A.; Dietrich, A. Model predictive control applied to different time-scale dynamics of flexible joint robots. *IEEE Rob. Autom. Lett.* **2023**, *8*, 672–679. [\[CrossRef\]](#)
- Zhu, Y.; Liu, J.; Yu, J.; Wang, Q.G. Command filtering-based adaptive fuzzy control of flexible-joint robots with time-varying full-state constraints. *IEEE Trans. Circuits Syst. II* **2024**, *71*, 682–686. [\[CrossRef\]](#)
- Xu, X.; Xu, S. Event-triggered adaptive neural tracking control of flexible-joint robot systems with input saturation. *IEEE Access* **2022**, *10*, 43367–43375. [\[CrossRef\]](#)
- Moyrón, J.; Moreno-Valenzuela, J.; Sandoval, J. Nonlinear PI “D”-type control of flexible joint robots by using motor position measurements is globally asymptotically stable. *IEEE Trans. Autom. Control* **2023**, *68*, 3648–3655. [\[CrossRef\]](#)
- Bu, X.; Qi, Q.; Jiang, B. A simplified finite-time fuzzy neural controller with prescribed performance applied to waverider aircraft. *IEEE Trans. Fuzzy Syst.* **2022**, *30*, 2529–2537. [\[CrossRef\]](#)
- Li, J.; Ma, K.; Wu, Z. Prescribed performance control for uncertain flexible-joint robotic manipulators driven by DC motors. *Int. J. Control Autom.* **2021**, *19*, 1640–1650. [\[CrossRef\]](#)
- Liu, L.; Yao, W.H.; Guo, Y. Prescribed performance tracking control of a free-flying flexible-joint space robot with disturbances under input saturation. *J. Franklin Inst.* **2021**, *358*, 4571–4601. [\[CrossRef\]](#)
- Ma, H.; Zhou, Q.; Li, H.; Lu, R. Adaptive prescribed performance control of a flexible-joint robotic manipulator with dynamic uncertainties. *IEEE Trans. Cybern.* **2022**, *52*, 12905–12915. [\[CrossRef\]](#)
- Atawnih, A.; Doulgeri, Z.; Rovithakis, G.A. Operational space prescribed tracking performance and compliance in flexible joint robots. *ASME J. Dyn. Syst. Meas. Control* **2015**, *137*, 074503. [\[CrossRef\]](#)
- Kim, D.; Koh, K.; Cho, G.R.; Zhang, L.Q. A robust impedance controller design for series elastic actuators using the singular perturbation theory. *IEEE/ASME Trans. Mechatronics* **2020**, *25*, 164–174. [\[CrossRef\]](#)
- Sun, T.; Liang, D.; Song, Y. Singular-perturbation-based nonlinear hybrid control of redundant parallel robot. *IEEE Trans. Ind. Electron.* **2018**, *65*, 3326–3336. [\[CrossRef\]](#)
- Chen, H.Y.; Dong, X.C.; Yang, Y.; Liu, J.T. Fixed-time tracking control for flexible joint manipulator with prescribed performance constraint. *IEEE Access* **2021**, *9*, 99388–99397. [\[CrossRef\]](#)
- Guo, K.; Zheng, D.D.; Li, J. Optimal bounded ellipsoid identification with deterministic and bounded learning gains: Design and application to Euler-Lagrange systems. *IEEE Trans. Cybern.* **2022**, *52*, 10800–10813. [\[CrossRef\]](#)
- Dai, W.; Zhang, L.; Fu, J.; Chai, T.; Ma, X. Dual-rate adaptive optimal tracking control for dense medium separation process using neural networks. *IEEE Trans. Neural Netw. Learn. Syst.* **2021**, *32*, 4202–4216. [\[CrossRef\]](#)
- Shen, J.; Khodak, M.; Talwalkar, A. Efficient architecture search for diverse tasks. *Adv. Neural Inf. Process. Syst.* **2022**, *35*, 16151–16164.
- Shen, J.; Yang, L.F. Theoretically principled deep RL acceleration via nearest neighbor function approximation. *Proc. AAAI Conf. Artif. Intell.* **2021**, *35*, 9558–9566. [\[CrossRef\]](#)
- Shen, J.; Li, L.; Dery, L.M.; Staten, C.; Khodak, M.; Neubig, G.; Talwalkar, A. Cross-modal fine-tuning: Align then refine. In Proceedings of the 40th International Conference on Machine Learning, Honolulu, HI, USA, 23–29 July 2023; Volume 202, pp. 31030–31056.
- Ioannou, P.A.; Sun, J. *Robust Adaptive Control*; Prentice-Hall, Inc.: Upper Saddle River, NJ, USA, 1996.
- Liu, Y.J.; Zeng, Q.; Tong, S.; Chen, C.P.; Liu, L. Actuator failure compensation-based adaptive control of active suspension systems with prescribed performance. *IEEE Trans. Ind. Electron.* **2020**, *67*, 7044–7053. [\[CrossRef\]](#)
- Yang, Q.; Zhang, F.; Sun, Q.; Wang, C. Dynamic learning from adaptive neural control for full-state constrained strict-feedback nonlinear systems. *Neural Netw.* **2024**, *170*, 596–609. [\[CrossRef\]](#)
- Rout, R.; Cui, R.; Yan, W. Sideslip-compensated guidance-based adaptive neural control of marine surface vessels. *IEEE Trans. Cybern.* **2022**, *52*, 2860–2871. [\[CrossRef\]](#)
- Pan, Y.; Guo, K.; Bobtsov, A.; Yang, C.; Yu, H. Composite error learning robot control using discontinuous Lyapunov analysis. *IEEE Trans. Autom. Control* **2023**, *69*, 1705–1712. [\[CrossRef\]](#)
- Patre, P.M.; MacKunis, W.; Johnson, M.; Dixon, W.E. Composite adaptive control for Euler–Lagrange systems with additive disturbances. *Automatica* **2010**, *46*, 140–147. [\[CrossRef\]](#)
- Zhang, H.; Zhou, X.; Wang, Z.; Yan, H.; Sun, J. Adaptive consensus-based distributed target tracking with dynamic cluster in sensor networks. *IEEE Trans. Cybern.* **2018**, *49*, 1580–1591. [\[CrossRef\]](#)
- Du, G.L.; Zhang, P.; Liu, X. Markerless human-manipulator interface using leap motion with interval Kalman filter and improved particle filter. *IEEE Trans. Ind. Inform.* **2016**, *12*, 694–704. [\[CrossRef\]](#)
- de Jesús Rubio, J.; Yu, W.; Ferreyra, A. Neural network training with optimal bounded ellipsoid algorithm. *Neural Comput. Appl.* **2009**, *18*, 623–631. [\[CrossRef\]](#)
- Ge, X.H.; Han, Q.L.; Wang, Z. A dynamic event-triggered transmission scheme for distributed set-membership estimation over wireless sensor networks. *IEEE Trans. Cybern.* **2019**, *49*, 171–183. [\[CrossRef\]](#)
- Alexander, P.; Andrey, P.; Vadim, A. *Attractive Ellipsoids in Robust Control*; Birkhauser: Boston, MA, USA, 2014.



29. Jorge, D.; Alexander, P. Dynamic sliding mode control design using attracting ellipsoid method. *Automatica* **2011**, *47*, 1467–1472.
30. Cao, L.Y.; Schwartz, H. A directional forgetting algorithm based on the decomposition of the information matrix. *Automatica* **2000**, *36*, 1725–1731. [[CrossRef](#)]
31. Ordaz, P.; Poznyak, A. ‘KL’-gain adaptation for attractive ellipsoid method. *IMA J. Math. Control. Inf.* **2015**, *32*, 447–469. [[CrossRef](#)]
32. Guo, K.; Zhang, Z.; Zheng, D.D.; Sun, J. Set-membership adaptive robot control with deterministically bounded learning gains. *IEEE Trans. Ind. Informat.* **2023**, *19*, 8564–8574. [[CrossRef](#)]
33. Zheng, D.D.; Xie, W.F.; Chai, T. Identification and trajectory tracking control of nonlinear singularly perturbed system. *IEEE Trans. Ind. Electron.* **2017**, *64*, 3737–3747. [[CrossRef](#)]
34. Zheng, D.D.; Xie, W.F.; Ren, X.; Na, J. Identification and control for singularly perturbed systems using multitime-scale neural networks. *IEEE Trans. Neural Netw. Learn. Syst.* **2017**, *28*, 321–333. [[CrossRef](#)] [[PubMed](#)]
35. Sun, W.; Su, S.; Xia, J.; Nguyen, V. Adaptive fuzzy tracking control of flexible-joint robots with full-state constraints. *IEEE Trans. Syst. Man Cybern. Syst.* **2019**, *49*, 2201–2209. [[CrossRef](#)]
36. Khalil, H.K. *Nonlinear Systems*, 3rd ed.; Prentice Hall: Upper Saddle River, NJ, USA, 2002.
37. Chang, Y.Z.; Daniel, R.W. On the adaptive control of flexible joint robots. *Automatica* **1992**, *28*, 969–974. [[CrossRef](#)]
38. Zhang, C.; Na, J.; Wu, J.; Chen, Q.; Huang, Y. Proportional-integral approximation-free control of robotic systems with unknown dynamics. *IEEE/ASME Trans. Mechatronics* **2021**, *26*, 2226–2236. [[CrossRef](#)]
39. Bechlioulis, C.P.; Rovithakis, G.A. Robust adaptive control of feedback linearizable MIMO nonlinear systems with prescribed performance. *IEEE Trans. Autom. Control* **2008**, *53*, 2090–2099. [[CrossRef](#)]
40. Guo, K.; Pan, Y.; Yu, H. Composite learning robot control with friction compensation: A neural network-based approach. *IEEE Trans. Ind. Electron.* **2019**, *66*, 7841–7851. [[CrossRef](#)]
41. Wu, Z.; Guo, J.; Liu, B.; Ni, J.; Bu, X. Composite learning adaptive dynamic surface control for uncertain nonlinear strict-feedback systems with fixed-time parameter estimation under sufficient excitation. *Int. J. Robust Nonlinear Control* **2021**, *31*, 5865–5889. [[CrossRef](#)]

**Disclaimer/Publisher’s Note:** The statements, opinions and data contained in all publications are solely those of the individual author(s) and contributor(s) and not of MDPI and/or the editor(s). MDPI and/or the editor(s) disclaim responsibility for any injury to people or property resulting from any ideas, methods, instructions or products referred to in the content.